Enhanced stability of charge and orbital order in $La_{0.78}Sr_{2.22}Mn_2O_7$

B. J. Campbell,* D. N. Argyriou,† J. F. Mitchell, and R. Osborn
Materials Science Division, Argonne National Laboratory, Argonne, Illinois 60439, USA

B. Ouladdiaf and C. D. Ling
Institute Laue-Langevin, Grenoble, Boîte Postale 156, 38042 Grenoble, France

(Received 9 July 2003; revised manuscript received 24 November 2003; published 4 March 2004)

Not only is zigzag charge and orbital (CO) order shown to be present in the highly doped ($x=0.61$) bilayered manganite system $La_{2-2x}Sr_{1+2x}Mn_2O_7$, it demonstrates an enhanced stability relative to the $x=0.5$ composition where the ordered state might be expected to have the lowest entropy. No magnetic-field dependence is observed up to 5.25 T. The CO ordering temperature also increases from 210 K at $x=0.5$ to 230 K, and the broad hysteretic conversion of the CO-ordered state to the *A*-type AF state at low temperatures is only partial. Phase reorganization in this hysteretic mixed-phase region is seen to involve an exponential time relaxation above $T=50$ K, while reorganization ceases below 50 K, apparently due to the thermally activated nature of the underlying dynamics.

DOI: 10.1103/PhysRevB.69.104403 PACS number(s): 75.47.Gk, 61.12.−q, 75.25.+z, 61.44.Fw

INTRODUCTION

In recent years, the perovskite manganites have been the subject of intense interest, both for their potential applications and a wealth of novel physical phenomena. The Mn e_g electrons profoundly influence the structural, magnetic, and transport properties of the manganites where subtle interactions amongst the spin, charge, and orbital degrees of freedom lead to complex phase diagrams as a function of temperature, magnetic field, and doping level (i.e., the fraction of Mn sites in the $4+$ oxidation state).[1] The layered manganites are structurally classified as Ruddlesden-Popper phases, and are of special interest due to the reduced dimensionality of the perovskite regions.

The bilayered $La_{2-2x}Sr_{1+2x}Mn_2O_7$ system has received considerable attention due to the presence of a ferromagnetic metallic (FM) state at compositions in the $0.32<x<0.40$ region,[2] which gives rise to a sharp colossal magnetoresistive (CMR) transition, as well as a variety of antiferromagnetic (AF) and spin-canted structures[3,4] extending from $0.3<x<1.0$. Long-range charge and orbital (CO) order have been observed at $x=0.5$, where there are equal numbers of e_g electrons and holes in the valence band.[5,6] The CO order observed at $x=0.5$ is commonly referred to as ''zigzag,'' ''checkerboard,'' or ''CE'' due to early predictions by Goodenough that the CE-AF spin ordering would be favored by a specific charge-orbital configuration comprised of a checkerboard arrangement of Mn^{3+} and Mn^{4+} sites that hosts diagonal zig-zag chains of occupied $d(3z^2-r^2)$ orbitals.[7]

Experimental evidence for this connection has been provided by x-ray and neutron diffraction experiments[8–10] on $La_{0.5}Ca_{0.5}MnO_3$, $LaSrMnO_4$, and $LaSr_2Mn_2O_7$. In the layered materials, this association must be qualified, as the original magnetic analogy does not specify the relationship between the orderings in adjacent layers, which has been clarified in more recent work for both the CO (Ref. 8) and magnetic[11] cases. Below $x=0.5$, no long-range CO order is observed in the $La_{2-2x}Sr_{1+2x}Mn_2O_7$ system, though quasistatic short-range CO correlations have been identified over a broad range of compositions between $x=0.32$ and $x=0.48$.[12–14] Short-range CO correlations of the CE type were very recently observed[15] at $x=0.4$, which were dynamic rather than static in nature, highlighting the relative instability of this configuration in the presence of excess Mn^{3+}.

The resistivity at $x=0.5$ shows a significant increase at the CO ordering temperature, $T_{CO}=210$ K, involving the localization of the e_g charge carriers and a cooperative structural distortion.[6,8] At decreasing temperatures, however, this trend is soon arrested by the onset of *A*-type AF order at $T_{N(A)}=170$ K.[8,16] The *A*-AF phase continues to grow and eventually results in the reentrant disappearance of CO order, accompanied by a drop in the resistivity. Recent theoretical efforts suggest that the *A*-type phase exhibits x^2-y^2 orbital order, while also being a double-exchange metal,[17,18] so that the carriers are delocalized, but restrict themselves to the preferred orbitals as they traverse the lattice. This effect has been referred to as orbital polarization.[19] While diffraction studies have uncovered no evidence of the breathing-mode distortions[20] that would arise in a charge-ordered x^2-y^2 orbital lattice, a maximum-entropy-method study[21] of the charge-density distribution in *A*-type $NdSr_2Mn_2O_7$, and a series of recent resonant x-ray scattering studies,[22,23] support the existence of x^2-y^2 orbital polarization in a charge-disordered *A*-AF state. The increased hopping within a double-exchange-dominated ferromagnetic sheet would provide for better electron transport than the CO state, though the AF coupling between sheets inhibits intersheet hopping.

Evidence of CO order[24,25] has also been reported for $x>0.5$, though it remains relatively unexplored. For $x>0.5$, one might expect CO order to lose ground against the competing *A*-AF state because the imperfect balance between mobile e_g electrons and holes raises the entropy of the CO-ordered state. However, the CO-ordered phase is observed to be stable across a wide range of compositions in three-dimensional perovskite manganites such as $La_{1-x}Ca_xMnO_3$ and $Pr_{1-x}Ca_xMnO_3$,[26,27] possibly due to partial rather than

 ©2004 The American Physical Society

TABLE I. Comparison of transition temperatures for $x=0.5$ and $x=0.6$.

x	T_{CO}	$T_{N(A)}$	T^*	$T_{N(CE)}$
0.5	210 K[a]	170 K[a]	75 K[b]	145 K[b]
0.6	230 K	180 K	55 K	145 K

[a]From Argyriou *et al.* (Ref. 8).
[b]From Kubota *et al.* (Ref. 16).

complete CO order. In the present work, we investigate the delicate balance between the competing CE-CO and *A*-AF phases at $x=0.61$. Specifically, we observe an increased CO-order transition temperature, incomplete conversion to the low-temperature *A*-type AF phase, and greater resistance to field melting.

EXPERIMENT

A 100 mg ($4\times4\times1$ mm) single-crystal sample of $La_{0.78}Sr_{2.22}Mn_2O_7$ was cut from a large boule prepared in a double-mirror floating-zone image furnace. Single-crystal neutron diffraction (SCND) experiments were carried out on the four-circle diffractometer at ILL beamline D10, without energy analysis. Data were collected over the temperature range from 2 to 300 K, using incident wavelengths of 2.36 Å (graphite 200) and 1.26 Å (Cu 200). Bragg intensities were measured with an area detector and integrated from multiple detector frames using the RACER software program.[28] Crystallographic analyses of the SCND data were performed using the GSAS software suite.[29] Single-crystal resistivity data were also collected over the range from 10 to 300 K using the standard four-probe technique.

RESULTS AND DISCUSSION

A. Temperature and field dependence

The first indicator of enhanced CO-order stability at $x=0.61$ is the fact that T_{CO} has increased to 230 K (see Table I and Fig. 1). We note that this transition temperature in a bulk crystal is somewhat different than the 280 K T_{CO} reported for $x=0.60$ grains by electron diffraction.[25] The CO-ordered phase appears at T_{CO} and develops rapidly until $T_{N(A)}$, at which point the onset of the competing *A*-type AF order begins to reverse the growth of CO order. The CO wave vector was observed to be incommensurate with $q=(\varepsilon,-\varepsilon,0)$ and $\varepsilon=0.21$, which is consistent with the trend $\varepsilon=(1-x)/2$ reported previously[25,30] for $La_{2-2x}Sr_{1+2x}Mn_2O_7$ and $La_{1-x}Sr_{1+x}MnO_4$. The incommensurate wave vector of the CO order has been observed to produce a stripelike contrast in TEM images.[25] We also observe that the CO-ordered phase hosts its magnetic companion structure, the CE-type antiferromagnetic arrangement, below $T_{N(CE)}$. CE-AF order was reported at $x=0.5$ by Kubota *et al.*[16] where it vanished at T^*, along with the CO order. In the present case, at $x=0.61$, both the CO and CE-AF orderings persist below T^*.

A second indicator of enhanced CO order is the incomplete conversion of the CO order to *A*-type antiferromagnetic order. In contrast to the nearly complete disappearance of the CO phase below T^* in the $x=0.5$ system,[3,5,6,8] the same transition at $x=0.61$ shows a large CO-ordered component all the way down to 2 K. In Fig. 1, the resistivity clearly exhibits a peak at $T_{N(A)}$, where the CO superlattice intensities are greatest, confirming that the transport behavior is linked to the rise and fall of the CO-ordered phase.

The transition from CO order to *A*-type antiferromagnetic order between $T_{N(A)}$ and $T^*=50$ K is hysteretic and very broad, consistent with a first order phase transition. This hysteresis is observed in both the CO and *A*-type components as well as in the resistivity. The transition at T^* marks the low-temperature limit of the hysteretic region and also appears to coincide with the steep upturn in resistivity. Careful transport studies throughout the region from $0.45<x<0.6$ also show a transition from hysteretic reentrant behavior to a low-temperature insulating state, which was referred to as a second low-temperature CO phase.[24] The present data show that the amount of CO order remains constant below T^*, and contain no evidence of the formation of a new CO phase at T^*, suggesting instead that the *A*-type phase becomes an antiferromagnetic insulator.

The melting of CO order under the influence of a magnetic field is a well-known feature of several CMR manganite systems.[31] In the case of $LaSrMn_2O_7$ ($x=0.5$), a field of 4.5 T was sufficient destroy the CO superlattice peaks at 180 K.[32] For $La_{0.78}Sr_{2.22}Mn_2O_7$ ($x=0.61$), however, no field dependence ($\mathbf{H}\|c$) was observed at 170 K up to 5.25 T (see Fig. 2), again indicating a greatly enhanced stability for the CO phase.

B. Parent structure

A crystallographic analysis of the parent nuclear structure, the CO-ordered superstructure, the *A*-type AF structure, and

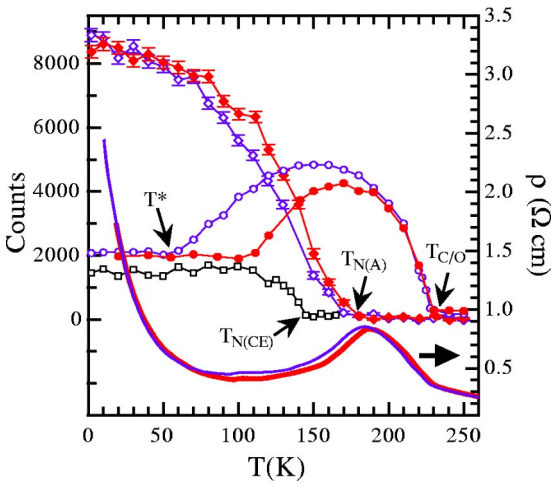

FIG. 1. The temperature dependence of the (1,1,1) peak intensity associated with *A*-type AF order (diamonds), the (1.79,2.21,0) satellite of the CO superstructure (circles), and the (1,0.5,2) peak associated with the weak CE-type AF order (squares). The CE-AF intensities have been multiplied by a factor of 20. Open symbols indicate a cooling cycle, while closed symbols indicate a warming cycle. The solid lines near the bottom are in-plane resistivity curves (upper trace is cooling cycle, lower is warming cycle).

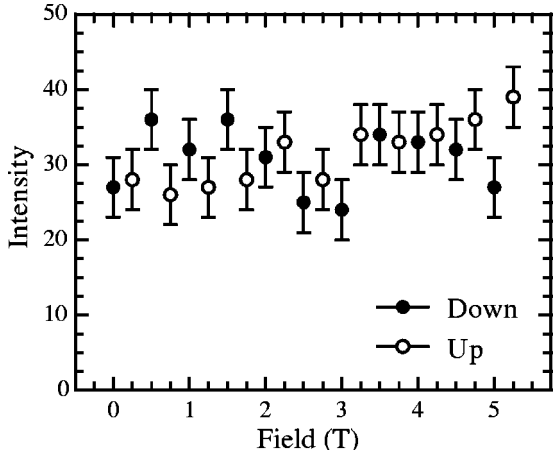

FIG. 2. Magnetic field dependence ($H\|c$) of the integrated (1.79,2.21,0) satellite peak intensity of the CO-ordered superstructure from $H=0$ to 5.25 T at 170 K. Open circles indicate increasing field strength, while closed circles indicate decreasing field strength. No field dependence is evident within the observed errors.

the CE-AF structure, was carried out using diffraction data collected at 2 K. The parent nuclear structure [$I4/mmm$, $a=3.854(2)$ Å, $c=19.940(5)$ Å] was refined using 307 reflections (174 unique) to obtain an $R_w(F^2)$ of 7.9%. Because the dimensions of the crystal were small ($4\times1\times1$ mm), no absorption correction was applied. The site occupancies of La and Sr were fixed based on the composition and assume no site preferences. Because anisotropic thermal parameters provided only a marginal improvement, isotropic thermal parameters were retained in the final refinement. The results appear in Table II.

C. Magnetic structure

In refining the two magnetic structures, it appeared fruitless to attempt to refine the moment, due to the presence of competing phases with unknown volume fractions. Instead, we estimated the moment based on the composition and refined the scale factor. By normalizing the measured intensities to the same monitor count, and comparing the scale factor to that of the nuclear structure refinement, an approximate volume fraction can be determined. The A-type AF phase consists of ferromagnetic sheets that are antiferromagnetically coupled within a single bilayer. Nearest-neighbor sheets from adjacent bilayers are aligned ferromagnetically, so as to make the overall structure anti-body-centered.[12] The ideal moment at 2 K, based on the composition, is $3.4\mu_B$/Mn. This value was fixed in the plane while the scale factor and a 90° moment-domain twin fraction were refined against 12 body-center violating reflections. The resulting fit [$R_w(F^2)=13.9\%$] exhibited a difference pattern that suggested that the AF moment direction is slightly tilted out of the plane. Adding this degree of freedom led to a much better fit [$R_w(F^2)=6.7\%$], and yielded an A-type AF moment that tilts 19(2)° out of the plane, as well as nearly equal portions of the two moment-domain twins. The resulting phase fraction was 75(6)%. Assuming a 100% phase fraction, and instead refining the moments, would yield $2.9(2)\mu_B$/Mn, which is somewhat larger than that reported from neutron powder diffraction data.[4] Differing amounts of a competing hysteretic ferromagnetic component, such as that reported by Li *et al.*,[25] could be responsible for the discrepancy.

TABLE II. Atomic coordinates and Mn-O bond lengths from the parent $I4/mmm$ structure refinement.

Site	z	$100\times u_{\rm iso}$ (Å^2)
La/Sr(1)	0.5	1.72(49)
La/Sr(2)	0.3181(1)	3.02(39)
Mn	0.0969(2)	2.94(61)
O1	0	8.52(74)
O2	0.1954(1)	8.19(54)
O3	0.0951(1)	6.58(40)
Mn−O1		1.932(2) Å
Mn−O2		1.964(4) Å
Mn−O3		1.927(0) Å

The CE-AF structure is generally associated with two distinct propagation vectors $\mathbf{q}_3=(1/4,1/4,0)$ and $\mathbf{q}_4=(0.5,0,0)$, which have been loosely associated with the magnetic ordering of Mn^{3+} and Mn^{4+} sublattices of the CO-ordered structure. While we do not argue in favor of complete charge disproportionation into discrete 3+ and 4+ Mn charge states, we do use these values as convenient site labels. Rather than assigning distinct moments to these sublattices, a nominal $3.4\mu_B$/Mn moment was assigned to each. The unit cell ($2\sqrt{2}a_0\times2\sqrt{2}a_0\times c$) contains eight Mn sites per perovskite sheet. After defining the moments within one perovskite sheet, the coupling along the c axis is antiferromagnetic within a single bilayer. When defining the moments in subsequent bilayers, there are two possible stacking schemes for the 4+ sublattice related by a 90° in-plane rotation. These produce identical intensities and have been treated as twin domains. Because there are six such stacking schemes for the 3+ sublattice, and because the 3+ sublattice satellite reflections are coincident with the CO-order superstructure satellites, we do not attempt to analyze the 3+ sublattice here.

The moments of the sublattice associated with wavevector $\mathbf{q}_4$ were analyzed first using 40 satellite reflections, to yield an $R_w(F^2)$ of 17.2%. The resulting phase fraction was 5.2(1)%, much smaller than the 75(6)% phase fraction of the A-type AF phase. Using the same scale factor, the intensities of the $\mathbf{q}_3$ satellite reflections were calculated and found to be roughly 30 times weaker than the coincident CO satellites, so that they effectively become lost in the noise, and may be neglected. While Kubota *et al.*[16] observed peaks at the half-integer l values along $(\frac{1}{4},\frac{1}{4},l)$, indicating the presence of some magnetic cell-doubling along the c axis, we observed none in our sample.

D. CO superstructure

The CO structure was examined using a small number of superlattice intensities (55 total, 37 unique, 29 with I/σ

>3) in the *Bbmm* space group symmetry ($a=\sqrt{2}a_0$, $b=2\sqrt{2}a_0$) as done in Ref. 8. This quadrupled-cell configuration effectively splits each crystallographically distinct site into two new sites. The in-plane Jahn-Teller distortions of the $Mn^{3+}-O_6$ octahedra at $x=0$ and $x=0.5$ cause the $Mn^{4+}O_6$ octahedra at $y=0.25$ and $y=0.75$ to shift cooperatively in the $+x$ and $-x$ directions, respectively. The small number of CO superstructure reflections measured were not sufficient for a comprehensive refinement, but do permit an estimate of the size of the JT distortion, relative to that reported for $x=0.5$.[8]

In order to make this estimate, we use the following approach. For $x=61\%$, isotropic thermal parameters and z parameters were set to the parent-structure values, and in-plane $Mn^{4+}O_6$ octahedral displacements were inserted into the model directly from Ref. 8 ($x=0.5$) and fixed so that only the scale factor and the x(La/Sr) displacements were refined. The structural modifications associated with an incommensurate wavevector were not determined or taken into account, and are presumably responsible for the high value of $R_w(F^2)=19\%$. The ratio of the volume-normalized scale factor (on F rather than F^2) to that of the parent-structure refined to 36(5)%. This value depends on both the participating phase fraction and on the overall displacement magnitudes.

We next invoke the reasonable assumption that the CE-AF fraction of the sample and the CO-ordered fraction are one and the same (i.e., 5.2%). While this volume fraction does depend on the nominal μ_B/Mn magnetic moments that were assigned, it is nevertheless a good estimate of the amount of CE-type material that survives below T^*. The magnitude of the CO-ordered superstructure displacements can then be estimated as $(\Delta_{JT,0.6}/\Delta_{JT,0.5})=36(5)\%\sqrt{[5.2(1)\%]}=1.6(2)$, which indicates a Jahn-Teller distortion of $1.6(2)\times 2.0(1)\%=3(1)\%$. The long and short Mn^{3+}-O bond lengths inferred from such a distortion at $x=0.61$ would be 1.962(12) Å and 1.901(12) Å. Recognizing that our estimate depends on several assumptions, we note that this larger distortion is similar to that reported in a powder diffraction study[9] of $La_{0.5}Ca_{0.5}MnO_3$, where the long and short JT-distorted Mn^{3+}-O bond lengths were 1.962(1) and 1.923(1) Å, respectively, and the JT distortion was (long-short)/long=2.0(1)%.

E. Time-dependent relaxation

The transition between *A*-type antiferromagnetic order and CE-type CO order is necessarily first order in nature, and therefore involves the hysteretic formation and migration of inter-phase interfaces. Upon cooling the sample slowly, the progress of the transition to the *A*-type phase halts at T^*, presumably due to a loss of phase-interface mobility. The dynamics that enable these interfaces to migrate appear to freeze out at T^*. The more persistent regions of CO-ordered material that survive down to T^* may benefit from inhomogeneously distributed lattice strains that stabilize the slightly lattice-mismatched[8] CE phase. Rewarming past 110 K then returns the system to the hysteresis curve that was interrupted upon reaching the ''persistent state'' at T^* during cooling.

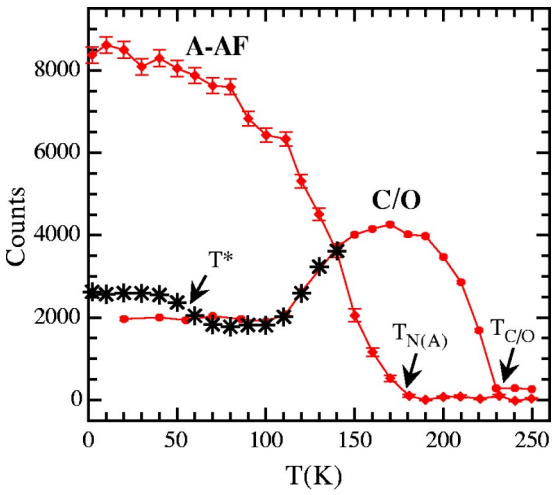

FIG. 3. Time and temperature dependence of the (1.79,2.21,0) satellite peak of the CO-ordered superstructure. Closed circles indicate a slow warming cycle that was preceded by a slow cooling cycle (0.3 K/min). Asterisks indicate a slow warming cycle that was preceded by rapid cooling (6 K/min) from 250 K and four days of holding time at 2 K. Closed diamonds indicate the development of the *A*-type AF phase on warming (from Fig. 2).

Upon rapidly cooling the system (~6 K/min) through the hysteretic region, from above $T_{N(A)}$ down to 2 K, the CO superstructure reflections are approximately 15% more intense than if the system had been cooled very slowly (0.3

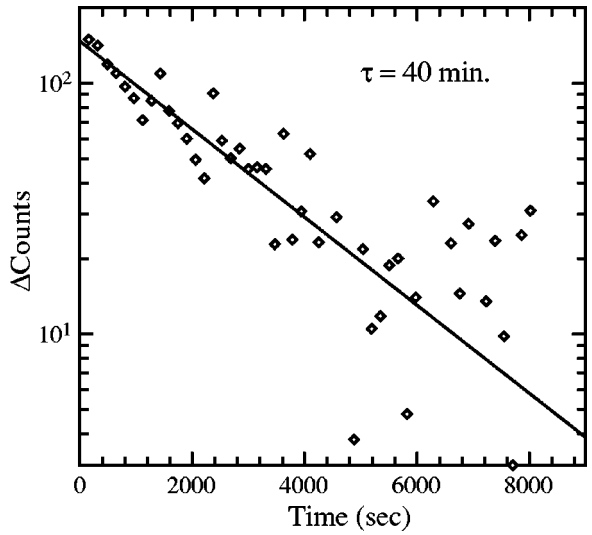

FIG. 4. Time dependence of the (1.79, 2.21, 0) satellite peak of the CO-ordered superstructure after rapid cooling (6 K/min) from 250 to 5 K, 90 min of holding time at 5 K, and very rapid reheating (25 K/min) to 70 K. The measurement began approximately 150 s after the heat was applied. The intensity decays exponentially towards a base level which has been subtracted from the data. Because the peak was integrated from a single area detector frame at each temperature, the data are not on the same scale as Figs. 1 and 2. The resulting decay constant is approximately 40 min.

K/min). Furthermore, reheating the sample to above 50 K causes the excess intensity to disappear, returning the system to the slowly cooled and warmed curve in Fig. 3. A measure of the dynamics of this process appears in Fig. 4. After rapidly cooling (6 K/min) to 5 K, and holding for 90 min, the temperature was quickly (25 K/min) raised to 70 K and held for 120 min. The relaxation to the persistent state was reasonably well-approximated by an exponential with a time constant of 40 min.

This rapid cooling from $T_{N(A)}$ where the CO-ordered phase is near its maximum appears to quench some of the more mobile interfaces in place, protecting weakly stabilized regions of CE material that should have been consumed by the *A*-AF phase in the persistent state. Warming the quenched system slowly up past T^* then restores mobility to these interfaces and permits the system to relax into the persistent state, with an associated loss of excess CO-ordered material and CO peak intensity.

CONCLUSIONS

Charge and orbital (CO) order are not only present at $x=0.61$, but exhibit an enhanced stability relative to the $x=0.5$ composition. The CO ordering temperature is increased and the broad hysteretic conversion of the CO-ordered state to the *A*-type AF state is halted at $T^*=50$ K, so that a significant CO-ordered component persists all the way down to 2 K. At 170 K, the CO order is shown to be unaffected by a 5.25 T magnetic field. At 2 K, the CO-ordered phase, which also hosts CE-AF order, has a volume fraction of about 5%, while the *A* type has a volume fraction of 75%. The fact that 20% of the material does not participate in long-range magnetic order at 2 K appears to signal the beginning of a crossover to the spin-disordered state observed in the $0.65<x<0.75$ range.[9] By equating the CE-AF and CO-ordered phase fractions, the magnitude of the atomic displacements that comprise the CO superstructure appear to be larger than previously realized, and much closer to the values reported for $La_{0.5}Ca_{0.5}MnO_3$ perovskite. An incommensurate $(0.21, -0.21, 0)$ wave vector suggests a CO superstructure with a strong composition dependence, though the structural details remain to be determined.

Below T^*, the CE-CO to *A*-AF kinetics become too slow to allow for phase reorganization. Rapid cooling below T^* effectively quenches in excess CO order, while rewarming above T^* permits relaxation to the persistent state with a time constant of 40 min. The observed T^* might be associated with the low-temperature metal-insulator transition reported previously throughout the $0.45<x<0.6$ region of the phase diagram.[24] Because the CO-ordered peak intensities are temperature independent below T^*, it appears that the *A*-type phase becomes insulating at low temperatures. The small fraction of CO-ordered material makes a percolative effect improbable.

ACKNOWLEDGMENTS

The authors gratefully acknowledge helpful discussions with K. E. Gray and G. McIntyre. This work was supported by the U.S. Department of Energy Office of Basic Science under Contract No. W-31-109-ENG-38.

*Present address: Dept. of Physics and Astronomy, Brigham Young University, Provo, UT 84602.
†Present address: Hahn-Meitner Institute, Berlin D-14109, Germany.

[1] Y. Tokura and N. Nagaosa, Science **288**, 462 (2000).
[2] T. Kimura, Y. Tomioka, H. Kuwahara, A. Asamitsu, M. Tamura, and Y. Tokura, Science **274**, 1698 (1996).
[3] M. Kubota, H. Fujioka, K. Hirota, K. Ohoyama, Y. Moritomo, K. Yoshizawa, and Y. Endoh, J. Phys. Soc. Jpn. **69**, 1606 (2000).
[4] C. D. Ling, J. E. Millburn, J. F. Mitchell, D. N. Argyriou, J. Linton, and H. N. Bordallo, Phys. Rev. B **62**, 15096 (2000).
[5] T. Kimura, R. Kumai, Y. Tokura, J. Q. Li, and Y. Matsui, Phys. Rev. B **58**, 11 081 (1998).
[6] J. Q. Li, Y. Matsui, T. Kimura, and Y. Tokura, Phys. Rev. B **57**, R3205 (1998).
[7] J. B. Goodenough, Phys. Rev. **100**, 564 (1955).
[8] D. N. Argyriou, H. N. Bordallo, B. J. Campbell, A. K. Cheetham, D. E. Cox, J. S. Gardner, K. Hanif, A. dos Santos, and G. F. Strouse, Phys. Rev. B **61**, 15 269 (2000).
[9] P. G. Radaelli, D. E. Cox, M. Marezio, and S.-W. Cheong, Phys. Rev. B **55**, 3015 (1997).
[10] B. J. Sternlieb, J. P. Hill, U. C. Wildgruber, G. M. Luke, B. Nachumi, Y. Moritomo, and Y. Tokura, Phys. Rev. Lett. **76**, 2169 (1996).
[11] P. D. Battle, D. E. Cox, M. A. Green, J. E. Millburn, L. E. Spring, P. G. Radaelli, M. J. Rosseinsky, and J. F. Vente, Chem. Mater. **9**, 1042 (1997).
[12] L. Vasiliu-Doloc, S. Rosenkranz, R. Osborn, S. K. Sinha, J. W. Lynn, J. Mesot, O. H. Seeck, G. Preosti, A. J. Fedro, and J. F. Mitchell, Phys. Rev. Lett. **83**, 4393 (1999).
[13] B. J. Campbell, R. Osborn, D. N. Argyriou, L. Vasiliu-Doloc, J. F. Mitchell, S. K. Sinha, U. Ruett, C. D. Ling, Z. Islam, and J. W. Lynn, Phys. Rev. B **65**, 014427 (2002).
[14] M. Kubota, Y. Oohara, K. Yoshizawa, H. Fujioka, K. Shimizu, K. Hirota, Y. Moritomo, and Y. Endoh, J. Phys. Soc. Jpn. **69**, 1986 (2000).
[15] D. N. Argyriou, J. W. Lynn, R. Osborn, B. J. Campbell, J. F. Mitchell, U. Ruett, H. N. Bordallo, A. Wildes, and C. D. Ling, Phys. Rev. Lett. **89**, 036401 (2002).
[16] M. Kubota, K. Yoshizawa, Y. Moritomo, H. Fujioka, K. Hirota, and Y. Endoh, J. Phys. Soc. Jpn. **68**, 2202 (1999).
[17] R. Maezono, S. Ishihara, and N. Nagaosa, Phys. Rev. B **58**, 11 583 (1998).
[18] S. Yunoki, T. Hotta, and E. Dagotto, Phys. Rev. Lett. **84**, 3714 (2000).
[19] T. Akimoto, Y. Moritomo, K. Ohoyama, S. Okamoto, S. Ishihara, S. Maekawa, and A. Nakamura, Phys. Rev. B **59**, R14 153 (1999).
[20] T. Mizokawa and A. Fujimori, Phys. Rev. B **56**, R493 (1997).
[21] M. Takata, E. Nishibori, K. Kato, M. Sakata, and Y. Moritomo, J. Phys. Soc. Jpn. **68**, 2190 (1999).
[22] M. v. Zimmermann, J. P. Hill, D. Gibbs, M. Blume, D. Casa, B. Keimer, Y. Murakami, Y. Tomioka, and Y. Tokura, Phys. Rev. Lett. **83**, 4872 (1999).

[23] Y. Murakami, H. Kawada, H. Kawata, M. Tanaka, T. Arima, Y. Moritomo, and Y. Tokura, Phys. Rev. Lett. **80**, 1932 (1998); Y. Wakabayashi, Y. Murakami, Y. Moritomo, I. Koyama, H. Nakao, T. Kiyama, T. Kimura, Y. Tokura, and N. Wakabayashi, J. Phys. Soc. Jpn. **70**, 1194 (2001).

[24] J. Dho, W. S. Kim, H. S. Choi, E. O. Chi, and N. H. Hur, J. Phys.: Condens. Matter **13**, 3655 (2001).

[25] J. Q. Li, C. Dong, L. H. Liu, and Y. M. Ni, Phys. Rev. B **64**, 174413 (2001).

[26] Y. Tokura, Y. Tomioka, H. Kuwahara, A. Asamitsu, Y. Moritomo, and M. Kasai, J. Appl. Phys. **79**, 5288 (1996).

[27] S.-W. Cheong and H. Y. Hwang, in *Colossal Magnetoresistive Oxides*, Advances in Condensed Matter Science Vol 2, edited by Y. Tokura (Gordon & Breach, London, 2000), p. 307.

[28] C. Wilkinson and G. McIntyre (unpublished).

[29] A. Larson and R. B. von Dreele, GSAS Manual, Los Alamos Report No. LAUR-86-748, Los Alamos National Laboratory, 1986.

[30] S. Larochelle, A. Mehta, N. Kaneko, P. K. Mang, A. F. Panchula, L. Zhou, J. Arthur, and M. Greven, Phys. Rev. Lett. **87**, 095502 (2001).

[31] Y. Tomioka, A. Aswamitsu, Y. Moritomo, H. Kuwahara, and Y. Tokura, Phys. Rev. Lett. **74**, 5198 (1995); H. Kuwahara, Y. Tomioka, A. Asamitsu, Y. Moritomo, and Y. Tokura, Science **270**, 961 (1995).

[32] D. N. Argyriou, T. Chatterji, and J. Brown (unpublished).